Available online at www.sciencedirect.com

ScienceDirect

Procedia IUTAM 22 (2017) 123 – 130

Procedia IUTAM

www.elsevier.com/locate/procedia

IUTAM Symposium on Nonlinear and Delayed Dynamics of Mechatronic Systems

Dynamics of cutting near double Hopf bifurcation

Tamás G. Molnár[a,*], Zoltán Dombóvári[a], Tamás Insperger[b], Gábor Stépán[a]

[a]*Department of Applied Mechanics, Budapest University of Technology and Economics, H-1111 Budapest, Hungary*
[b]*Department of Applied Mechanics, Budapest University of Technology and Economics and MTA-BME Lendület Human Balancing Research Group, H-1111 Budapest, Hungary*

Abstract

Bifurcation analysis of the orthogonal cutting model with cutting force nonlinearity is presented with special attention to double Hopf bifurcations. The normal form of the system in the vicinity of the double Hopf point is derived analytically by means of center manifold reduction. The dynamics is restricted to a four-dimensional center manifold, and the long-term behavior is illustrated on simplified phase portraits in two dimensions. The topology of the phase portraits reveal the coexistence of periodic and quasi-periodic solutions, which are computed by approximate analytical formulas.

Peer-review under responsibility of organizing committee of the IUTAM Symposium on Nonlinear and Delayed Dynamics of Mechatronic Systems

Keywords: machine tool vibrations, nonlinearity, Hopf bifurcation, double Hopf bifurcation, center manifold reduction

1. Introduction

The theory of surface regeneration has been widely used since the 1950's to explain self-excited vibrations in metal cutting [1,2]. According to the theory, the vibrations of the machine tool copy onto the workpiece during cutting and hence affect the vibrations at the subsequent cut. Therefore, regenerative machine tool vibrations (or machine tool chatter) can be described by differential equations with time delay. The equations are typically nonlinear due to nonlinear cutting force expressions [3,4,5,6].

It is well-known that time delay often leads to the instability of dynamical systems. In the nonlinear models of machining (turning), the stability of stationary cutting is lost via Hopf bifurcation. Hopf bifurcation can be investigated either by analytical methods, such as the center manifold reduction [7,8,9] or the method of multiple scales [10,11,12], or by numerical bifurcation analysis [13].

At the intersections of the stability boundaries associated with Hopf bifurcation, codimension-two double Hopf bifurcations take place. Double Hopf bifurcation gives rise to rich dynamics and complex behavior in dynamic systems [14,15,16,17,18,19,20,21,22,23]. The double Hopf bifurcation in orthogonal cutting has been analyzed in [24] by the method of multiple scales. Here, we dedicate this paper to the analysis of the double Hopf bifurcation in cutting by means of center manifold reduction.

* Corresponding author.
E-mail address: molnar@mm.bme.hu

Peer-review under responsibility of organizing committee of the IUTAM Symposium on Nonlinear and Delayed Dynamics of Mechatronic Systems
doi:10.1016/j.piutam.2017.08.016

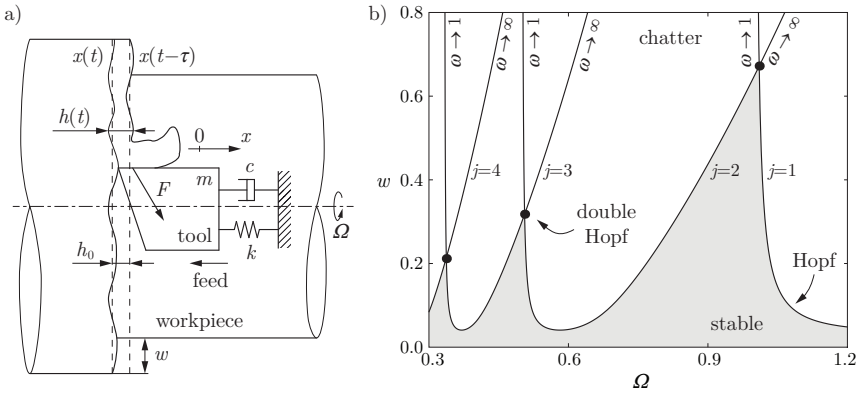

Fig. 1. Single-degree-of-freedom mechanical model of orthogonal cutting (a); the corresponding stability lobe diagram (b).

2. Mechanical model, stability, and bifurcations

Consider the single-degree-of-freedom mechanical model of orthogonal cutting shown in Fig. 1(a). The workpiece is assumed to be rigid, rotating with dimensionless angular velocity Ω. The tool is assumed to be compliant in the feed direction, and is modeled by a mass-spring-damper system. The dimensionless equation governing the tool's motion relative to the workpiece can be given in the form [9]

$$\ddot{x}(t) + 2\zeta\dot{x}(t) + x(t) = w\Big((x(t-\tau) - x(t)) + \eta_2 (x(t-\tau) - x(t))^2 + \eta_3 (x(t-\tau) - x(t))^3 \Big), \tag{1}$$

where t is the dimensionless time (scaled by the natural angular frequency of the system), x is the dimensionless tool position (scaled by the feed h_0 per revolution), and ζ is the damping ratio. The right-hand side of Eq. (1) yields the x-directional component of the cutting force variation, which is proportional to the dimensionless chip width w and is a cubic polynomial of the dimensionless chip thickness variation $x(t-\tau) - x(t)$ [3]. Parameters η_2 and η_3 denote dimensionless quadratic and cubic cutting-force coefficients, whereas $\tau = 2\pi/\Omega$ is called regenerative delay, which is equal to the period of workpiece rotations.

The equivalent first-order representation of the second-order system (1) reads

$$\mathbf{y}'(t) = \mathbf{L}\mathbf{y}(t) + \mathbf{R}\mathbf{y}(t-\tau) + \mathbf{g}(\mathbf{y}_t)\,. \tag{2}$$

The vector $\mathbf{y}$ of state variables, the linear and retarded coefficient matrices $\mathbf{L}$ and $\mathbf{R}$, and the nonlinear term $\mathbf{g}$ are defined by

$$\mathbf{y}(t) = \begin{bmatrix} x(t) \\ \dot{x}(t) \end{bmatrix}, \quad \mathbf{L} = \begin{bmatrix} 0 & 1 \\ -(1+w) & -2\zeta \end{bmatrix}, \quad \mathbf{R} = \begin{bmatrix} 0 & 0 \\ w & 0 \end{bmatrix}, \quad \mathbf{g}(\mathbf{y}_t) = \begin{bmatrix} 0 \\ w\Big(\eta_2 (y_1(t-\tau) - y_1(t))^2 + \eta_3 (y_1(t-\tau) - y_1(t))^3\Big) \end{bmatrix}, \tag{3}$$

where subscript 1 refers to the first component of a vector, $y_1(t) = x(t)$.

2.1. Hopf bifurcation

The equilibrium $x(t) \equiv 0$ of Eq. (1) corresponds to stationary cutting with uniform prescribed chip thickness h_0. Machine tool vibrations are associated with the loss of stability of this equilibrium. The linear stability of the solution $x(t) \equiv 0$ is determined by the real part of the characteristic exponents of system (2), which are the roots of the characteristic equation

$$D(\lambda) = \det\left(\lambda\mathbf{I} - \mathbf{L} - \mathbf{R}\mathrm{e}^{-\lambda\tau}\right) = \lambda^2 + 2\zeta\lambda + 1 + w\left(1 - \mathrm{e}^{-\lambda\tau}\right) = 0\,. \tag{4}$$

The equilibrium related to stationary cutting is linearly stable provided that all the infinitely many characteristic exponents are located in the left half of the complex plane. Along the stability boundaries of the system, a pair of

complex conjugate characteristic exponents $\lambda = \pm \mathrm{i}\omega$ ($\mathrm{i}^2 = -1, \omega \leq 0$) lies on the imaginary axis. Correspondingly, the real and imaginary parts of $D(\mathrm{i}\omega) = 0$ give the stability boundaries (or stability lobes) in the form[9]

$$w_{\mathrm{H}}(\omega) = \frac{\left(\omega^2 - 1\right)^2 + 4\zeta^2\omega^2}{2\left(\omega^2 - 1\right)}, \quad \tau_{\mathrm{H}}(j,\omega) = \frac{2}{\omega}\left(j\pi - \arctan\left(\frac{\omega^2 - 1}{2\zeta\omega}\right)\right), \quad \Omega_{\mathrm{H}}(j,\omega) = \frac{2\pi}{\tau_{\mathrm{H}}(j,\omega)}, \tag{5}$$

where $j \in \mathbb{Z}$ is the lobe number. The stability boundaries are often depicted in the plane (Ω, w) of the angular velocity and the chip width, resulting in so-called stability lobe diagrams, see Fig. 1(b) for $\zeta = 0.02$.

Along the stability boundaries (5), a Hopf bifurcation takes place – note that a fold bifurcation cannot happen in system (1). For the analysis of the Hopf bifurcation, the reader is referred to[8,9,11,12]. According to[9], the sense of the Hopf bifurcation is subcritical at each point of the stability lobes (5) for real-life cutting-force parameters η_2, η_3. The subcritical Hopf bifurcation gives rise to an unstable periodic solution in the vicinity of the equilibrium. The approximate angular frequency of the periodic solution is ω.

2.2. Double Hopf bifurcation

Hereinafter we use previous results[9] for the Hopf bifurcation, and extend them to analyze the double Hopf bifurcation in system (1). According to Fig. 1(b), the stability boundaries associated with Hopf bifurcation intersect at some points. At the intersection point of two lobes with lobe numbers j_1 and j_2, two periodic solutions are born simultaneously with angular frequencies ω_1 and ω_2, respectively. In such points, a double Hopf bifurcation takes place, which even gives rise to a quasi-periodic solution with two angular frequencies ω_1 and ω_2[25]. The double Hopf bifurcation points and the two angular frequencies are given by $w_{\mathrm{dH}} = w_{\mathrm{H}}(\omega_1) = w_{\mathrm{H}}(\omega_2)$ and $\Omega_{\mathrm{dH}} = \Omega_{\mathrm{H}}(\omega_1) = \Omega_{\mathrm{H}}(\omega_2)$ and Eq. (5).

In what follows, we analyze the double Hopf bifurcation by determining the normal form of the system by means of center manifold reduction, in order to find approximate expressions for the arising periodic and quasi-periodic solutions. We choose Ω and w as bifurcation parameters for the analysis of this codimension-two bifurcation.

3. Center manifold reduction and normal form calculations

The normal form of system (1) in the vicinity of the double Hopf bifurcation point $(\Omega_{\mathrm{dH}}, w_{\mathrm{dH}})$ can be determined by means of the method of multiple scales[24], or by means of center manifold reduction. Here, we use the latter for normal form analysis. The theory of center manifold reduction is discussed in[7], whereas its application to Hopf and double Hopf bifurcations can be found for example in[8,9,14,17,18,21,22].

The main idea behind center manifold reduction is the following. The phase space of the time-delay system (1) is infinite-dimensional, as it has infinitely many characteristic exponents satisfying Eq. (4). At the double Hopf bifurcation point, four characteristic exponents $\pm\mathrm{i}\omega_{1,2}$ are located on the imaginary axis, while the other infinitely many exponents lie in the left-half plane. Therefore, in the vicinity of the double Hopf bifurcation, there exists a four-dimensional center manifold embedded in the infinite-dimensional phase space, which attracts the solutions of the time-delay system. The flow on this center manifold determines the long-term dynamics of the system. The long-term behavior can be investigated by restricting the dynamics to the four-dimensional center manifold, and analyzing a four-dimensional system of ordinary differential equations instead of the infinite-dimensional delay-differential equation.

3.1. Restriction to the center manifold

The restriction to the center manifold can be done according to the decomposition theorem in Chapter 7.3 of the book by Hale[7]. In order to carry out the decomposition, we rewrite Eq. (2) in operator differential equation form

$$\dot{\mathbf{y}}_t(\theta) = \left(\mathcal{A}\mathbf{y}_t\right)(\theta) + \left(\mathcal{F}(\mathbf{y}_t)\right)(\theta), \tag{6}$$

where $\mathbf{y}_t \in \mathcal{H} : [-\tau, 0] \to \mathbb{R}^2$, $\mathbf{y}_t(\theta) = \mathbf{y}(t+\theta)$ is the state of the system in the Hilbert space $\mathcal{H}$ of continuously differentiable vector-valued functions. The linear and the nonlinear operators $\mathcal{A}, \mathcal{F} : \mathcal{H} \to \mathcal{H}$ are defined by

$$\left(\mathcal{A}\mathbf{u}\right)(\theta) = \begin{cases} \mathbf{u}'(\theta) & \text{if } \theta \in [-\tau, 0), \\ \mathbf{L}\mathbf{u}(0) + \mathbf{R}\mathbf{u}(-\tau) & \text{if } \theta = 0, \end{cases} \qquad \left(\mathcal{F}(\mathbf{u})\right)(\theta) = \begin{cases} \mathbf{0} & \text{if } \theta \in [-\tau, 0), \\ \mathbf{g}(\mathbf{u}) & \text{if } \theta = 0. \end{cases} \tag{7}$$

Furthermore, we introduce operator $\mathcal{A}^* : \mathcal{H}^* \to \mathcal{H}^*$, which is formally adjoint to operator $\mathcal{A}$ relative to a certain bilinear form. The formal adjoint satisfies $(\mathbf{v}, \mathcal{A}\mathbf{u}) = (\mathcal{A}^*\mathbf{v}, \mathbf{u})$ for any pair of $\mathbf{u} \in \mathcal{H} : [-\tau, 0] \to \mathbb{R}^2$ and $\mathbf{v} \in \mathcal{H}^* : [0, \tau] \to \mathbb{R}^2$, where $\mathcal{H}^*$ is the adjoint space, and operation $(\ ,\ ) : \mathcal{H}^* \times \mathcal{H} \to \mathbb{R}$ indicates a bilinear form. According to Eqs. (3.1) and (3.3) in Chapter 7.3 of Hale's book[7], the definition of the formal adjoint and the bilinear form become

$$(\mathcal{A}^*\mathbf{v})(\varphi) = \begin{cases} -\mathbf{v}'(\varphi) & \text{if } \varphi \in (0, \tau], \\ \mathbf{L}^{\mathsf{H}}\mathbf{v}(0) + \mathbf{R}^{\mathsf{H}}\mathbf{v}(\tau) & \text{if } \varphi = 0, \end{cases} \qquad (\mathbf{u}, \mathbf{v}) = \mathbf{u}^{\mathsf{H}}(0)\mathbf{v}(0) + \int_0^\tau \mathbf{u}^{\mathsf{H}}(\varphi)\mathbf{R}\mathbf{v}(\varphi - \tau)\mathrm{d}\varphi, \tag{8}$$

where the superscript H of $\mathbf{R}$, $\mathbf{L}$, and $\mathbf{u}$ refers to conjugate transpose.

The four-dimensional center manifold is tangent to the eigenfunctions (infinite-dimensional eigenvectors) $\mathbf{s}^k(\theta)$ and $\overline{\mathbf{s}}^k(\theta)$ $(k = 1, 2)$ of operator $\mathcal{A}$ at $(\Omega_{\mathrm{dH}}, w_{\mathrm{dH}})$. Whereas restriction to the center manifold can be performed using the eigenfunctions $\mathbf{n}^k(\varphi)$ and $\overline{\mathbf{n}}^k(\varphi)$ $(k = 1, 2)$ of operator $\mathcal{A}^*$ at $(\Omega_{\mathrm{dH}}, w_{\mathrm{dH}})$. The eigenfunctions are defined by

$$\left(\mathcal{A}\mathbf{s}^k\right)(\theta) = \mathrm{i}\omega_k\mathbf{s}^k(\theta), \qquad \left(\mathcal{A}\overline{\mathbf{s}}^k\right)(\theta) = -\mathrm{i}\omega_k\overline{\mathbf{s}}^k(\theta), \tag{9}$$

$$\left(\mathcal{A}^*\mathbf{n}^k\right)(\varphi) = -\mathrm{i}\omega_k\mathbf{n}^k(\varphi), \quad \left(\mathcal{A}^*\overline{\mathbf{n}}^k\right)(\varphi) = \mathrm{i}\omega_k\overline{\mathbf{n}}^k(\varphi), \tag{10}$$

where over-bar denotes complex conjugate. After solving the boundary value problems (9) and (10), the eigenfunctions are obtained in the form $\mathbf{s}^k(\theta) = \mathbf{s}^k_{\mathrm{R}}(\theta) + \mathrm{i}\mathbf{s}^k_{\mathrm{I}}(\theta)$, $\mathbf{n}^k(\varphi) = \mathbf{n}^k_{\mathrm{R}}(\varphi) + \mathrm{i}\mathbf{n}^k_{\mathrm{R}}(\varphi)$,

$$\begin{aligned} \mathbf{s}^k_{\mathrm{R}}(\theta) &= \begin{bmatrix} \cos(\omega_k\theta) \\ -\omega_k\sin(\omega_k\theta) \end{bmatrix}, \quad \mathbf{n}^k_{\mathrm{R}}(\varphi) = \frac{2}{p_k^2+q_k^2}\begin{bmatrix} (2\zeta p_k + \omega_k q_k)\cos(\omega_k\varphi) + (\omega_k p_k - 2\zeta q_k)\sin(\omega_k\varphi) \\ p_k\cos(\omega_k\varphi) - q_k\sin(\omega_k\varphi) \end{bmatrix}, \\ \mathbf{s}^k_{\mathrm{I}}(\theta) &= \begin{bmatrix} \sin(\omega_k\theta) \\ \omega_k\cos(\omega_k\theta) \end{bmatrix}, \quad \mathbf{n}^k_{\mathrm{I}}(\varphi) = \frac{2}{p_k^2+q_k^2}\begin{bmatrix} (-\omega_k p_k + 2\zeta q_k)\cos(\omega_k\varphi) + (2\zeta p_k + \omega_k q_k)\sin(\omega_k\varphi) \\ q_k\cos(\omega_k\varphi) + p_k\sin(\omega_k\varphi) \end{bmatrix}, \end{aligned} \tag{11}$$

where the constants p_k and q_k are given by Eq. (A.1) in Appendix A. Note that the eigenfunctions satisfy the orthonormality conditions $(\mathbf{n}^1_{\mathrm{R}}, \mathbf{s}^1_{\mathrm{R}}) = 1$, $(\mathbf{n}^1_{\mathrm{R}}, \mathbf{s}^1_{\mathrm{I}}) = 0$, $(\mathbf{n}^2_{\mathrm{R}}, \mathbf{s}^2_{\mathrm{R}}) = 1$, and $(\mathbf{n}^2_{\mathrm{R}}, \mathbf{s}^2_{\mathrm{I}}) = 0$.

Using these eigenfunctions and the decomposition theorem in Hale's book[7], the phase space of the time-delay system (6) can be decomposed into stable and center subspaces as

$$\mathbf{y}_t(\theta) = z_1(t)\mathbf{s}^1_{\mathrm{R}}(\theta) + z_2(t)\mathbf{s}^1_{\mathrm{I}}(\theta) + z_3(t)\mathbf{s}^2_{\mathrm{R}}(\theta) + z_4(t)\mathbf{s}^2_{\mathrm{I}}(\theta) + \mathbf{y}_{tn}(\theta), \tag{12}$$

where $z_1(t)$, $z_2(t)$, $z_3(t)$ and $z_4(t)$ are coordinates aligned with the center manifold that describe the long-term dynamics of the time-delay system (1), while $\mathbf{y}_{tn}(\theta)$ represents the infinite-dimensional stable subsystem transverse to the center manifold. According to the decomposition theorem, the formulas of these components read

$$\begin{aligned} &z_1(t) = (\mathbf{n}^1_{\mathrm{R}}, \mathbf{y}_t), \quad z_2(t) = (\mathbf{n}^1_{\mathrm{I}}, \mathbf{y}_t), \quad z_3(t) = (\mathbf{n}^2_{\mathrm{R}}, \mathbf{y}_t), \quad z_4(t) = (\mathbf{n}^2_{\mathrm{I}}, \mathbf{y}_t), \\ &\mathbf{y}_{tn}(\theta) = \mathbf{y}_t(\theta) - z_1(t)\mathbf{s}^1_{\mathrm{R}}(\theta) - z_2(t)\mathbf{s}^1_{\mathrm{I}}(\theta) - z_3(t)\mathbf{s}^2_{\mathrm{R}}(\theta) - z_4(t)\mathbf{s}^2_{\mathrm{I}}(\theta). \end{aligned} \tag{13}$$

Differentiating Eq. (13) with respect to time, using Eqs. (6), (12), (9), and omitting the arguments t, θ we get

$$\begin{aligned} \begin{bmatrix} \dot{z}_1 \\ \dot{z}_2 \\ \dot{z}_3 \\ \dot{z}_4 \\ \dot{\mathbf{y}}_{tn} \end{bmatrix} &= \begin{bmatrix} 0 & \omega_1 & 0 & 0 & \mathcal{O} \\ -\omega_1 & 0 & 0 & 0 & \mathcal{O} \\ 0 & 0 & 0 & \omega_2 & \mathcal{O} \\ 0 & 0 & -\omega_2 & 0 & \mathcal{O} \\ \mathfrak{o} & \mathfrak{o} & \mathfrak{o} & \mathfrak{o} & \mathcal{A} \end{bmatrix}\begin{bmatrix} z_1 \\ z_2 \\ z_3 \\ z_4 \\ \mathbf{y}_{tn} \end{bmatrix} + \begin{bmatrix} n^1_{\mathrm{R}2}(0)\mathcal{F}_2(0) \\ n^1_{\mathrm{I}2}(0)\mathcal{F}_2(0) \\ n^2_{\mathrm{R}2}(0)\mathcal{F}_2(0) \\ n^2_{\mathrm{I}2}(0)\mathcal{F}_2(0) \\ \mathcal{G}(\mathbf{y}_t) \end{bmatrix}, \\ \mathcal{G}(\mathbf{y}_t) &= \mathcal{F}(\mathbf{y}_t) - \mathcal{F}_2(0)\left(n^1_{\mathrm{R}2}(0)\mathbf{s}^1_{\mathrm{R}} + n^1_{\mathrm{I}2}(0)\mathbf{s}^1_{\mathrm{I}} + n^2_{\mathrm{R}2}(0)\mathbf{s}^2_{\mathrm{R}} + n^2_{\mathrm{I}2}(0)\mathbf{s}^2_{\mathrm{I}}\right) \end{aligned} \tag{14}$$

where $\mathfrak{o} : \mathbb{R} \to \mathcal{H}$ is a zero operator, $\mathcal{O} : \mathcal{H} \to \mathbb{R}$ is a zero functional, subscript 2 indicates the second component of vectors, and $\mathcal{F}_2(0)$ shortly indicates the second component of $\mathcal{F}(\mathbf{y}_t)$ at $\theta = 0$ with $\Omega = \Omega_{\mathrm{dH}}$ and $w = w_{\mathrm{dH}}$. Note that in Eq. (14), the four-dimensional center subsystem is already decoupled on the linear level from the infinite-dimensional stable subsystem.

In order to decouple the nonlinear terms in the equations for z_1, z_2, z_3, z_4, the dynamics must be restricted to the four-dimensional center manifold $\mathbf{y}_m(\theta) = \mathbf{y}_m^{\mathrm{CM}}(z_1, z_2, z_3, z_4)(\theta)$. Second-order approximation of the center manifold allows us to decouple the nonlinear terms up to third order in Eq. (14):

$$\mathbf{y}_m^{\mathrm{CM}}(z_1, z_2, z_3, z_4)(\theta) \approx \frac{1}{2}\Big(\mathbf{h}_{11}(\theta)z_1^2 + \mathbf{h}_{22}(\theta)z_2^2 + \mathbf{h}_{33}(\theta)z_3^2 + \mathbf{h}_{44}(\theta)z_4^2 + 2\mathbf{h}_{12}(\theta)z_1z_2 + 2\mathbf{h}_{13}(\theta)z_1z_3 + 2\mathbf{h}_{14}(\theta)z_1z_4 + 2\mathbf{h}_{23}(\theta)z_2z_3 + 2\mathbf{h}_{24}(\theta)z_2z_4 + 2\mathbf{h}_{34}(\theta)z_3z_4\Big), \quad (15)$$

where the coefficients $\mathbf{h}_{mn}(\theta)$ $(m, n = 1, 2, 3, 4,\ m \le n)$ can be calculated by solving a boundary value problem defined by Eqs. (14) and (15). Restricting the dynamics to the center manifold, using the second-order approximation (15) of the center manifold and the third-order approximation of the nonlinearities in Eq. (14), we get a four-dimensional decoupled set of ordinary differential equations in the form

$$\begin{bmatrix} \dot{z}_1 \\ \dot{z}_2 \\ \dot{z}_3 \\ \dot{z}_4 \end{bmatrix} = \begin{bmatrix} 0 & \omega_1 & 0 & 0 \\ -\omega_1 & 0 & 0 & 0 \\ 0 & 0 & 0 & \omega_2 \\ 0 & 0 & -\omega_2 & 0 \end{bmatrix} \begin{bmatrix} z_1 \\ z_2 \\ z_3 \\ z_4 \end{bmatrix} + \begin{bmatrix} G_1(z_1, z_2, z_3, z_4) \\ G_2(z_1, z_2, z_3, z_4) \\ G_3(z_1, z_2, z_3, z_4) \\ G_4(z_1, z_2, z_3, z_4) \end{bmatrix}. \quad (16)$$

Here, $G_{1,2,3,4}$ are functions with purely quadratic and cubic nonlinearities. Hence Eq. (16) gives a third-order approximation of the center subsystem, which is suitable for normal form calculations and bifurcation analysis[25].

3.2. Normal form in the vicinity of the double Hopf point

The four-dimensional system (16) can be written in polar form with amplitudes r_1, r_2 and phase angles θ_1, θ_2 as[25]

$$\begin{aligned} \dot{r}_1 &= \mu_1 r_1 + a_{11}r_1^3 + a_{12}r_1r_2^2, \quad \dot{\theta}_1 = \omega_1 + c_{11}r_1^2 + c_{12}r_2^2, \\ \dot{r}_2 &= \mu_2 r_2 + a_{21}r_1^2r_2 + a_{22}r_2^3, \quad \dot{\theta}_2 = \omega_2 + c_{21}r_1^2 + c_{22}r_2^2, \end{aligned} \quad (17)$$

where the constants a_{mn} and c_{mn} $(m, n = 1, 2)$ can be obtained by the formulas given in[26]. Accordingly, periodic and quasi-periodic orbits arise, which can be approximated by $r_1\cos(\omega_1 t) + r_2\cos(\omega_2 t)$. In this paper, we focus only on the amplitude of the arising periodic and quasi-periodic solutions, hence we compute r_1 and r_2 only, for which the cubic coefficients a_{mn} are listed in Eq. (A.2) of Appendix A. The coefficients μ_1 and μ_2 of the linear terms are

$$\mu_1 = \gamma_{11}\hat{w} + \gamma_{12}\hat{\Omega}, \quad \mu_2 = \gamma_{21}\hat{w} + \gamma_{22}\hat{\Omega}, \quad (18)$$

where $\hat{\Omega} = \Omega - \Omega_{\mathrm{dH}}$ and $\hat{w} = w - w_{\mathrm{dH}}$ are the bifurcation parameters shifted to the double Hopf point. Whereas γ_{k1} and γ_{k2} $(k = 1, 2)$ are the root tendencies obtained by implicit differentiation of Eq. (4):

$$\gamma_{k1} = \mathrm{Re}\left(\frac{\partial\lambda}{\partial w}\Big|_{\lambda=\mathrm{i}\omega_k}\right) = \frac{p_kV_k + q_kW_k}{p_k^2 + q_k^2}, \quad \gamma_{k2} = \mathrm{Re}\left(\frac{\partial\lambda}{\partial\Omega}\Big|_{\lambda=\mathrm{i}\omega_k}\right) = w_{\mathrm{dH}}\frac{\tau_{\mathrm{dH}}^2}{2\pi}\omega_k\frac{q_k(V_k+1) - p_kW_k}{p_k^2 + q_k^2}, \quad (19)$$

with parameters listed in Eq. (A.1) of Appendix A.

4. Results and discussion

The analysis of the polar-form system (17) can be found in[25]. Accordingly, the long-term dynamics near the double Hopf point is determined by the parameters $a = a_{11}/|a_{11}|$, $b = a_{12}/|a_{22}|$, $c = a_{21}/|a_{11}|$, $d = a_{22}/|a_{22}|$, and $A = ad - bc$. The values of the bifurcation parameters, the chatter frequencies, the root tendencies, and the normal form coefficients at the first five double Hopf bifurcation points are listed in Tab. 1 for $\eta_2 = 1.43059$ and $\eta_3 = 0.738487$, which are dimensionless parameters corresponding to measured cutting-force coefficients[3] and feed per revolution $h_0 = 250\,\mu$m. The coefficients b and c have also been computed numerically by DDE-Biftool[13], and they agree with the analytical results (see b_{num}, c_{num}). According to the table, a, b, c, and d are always positive, whereas $A > 0$ holds for the first

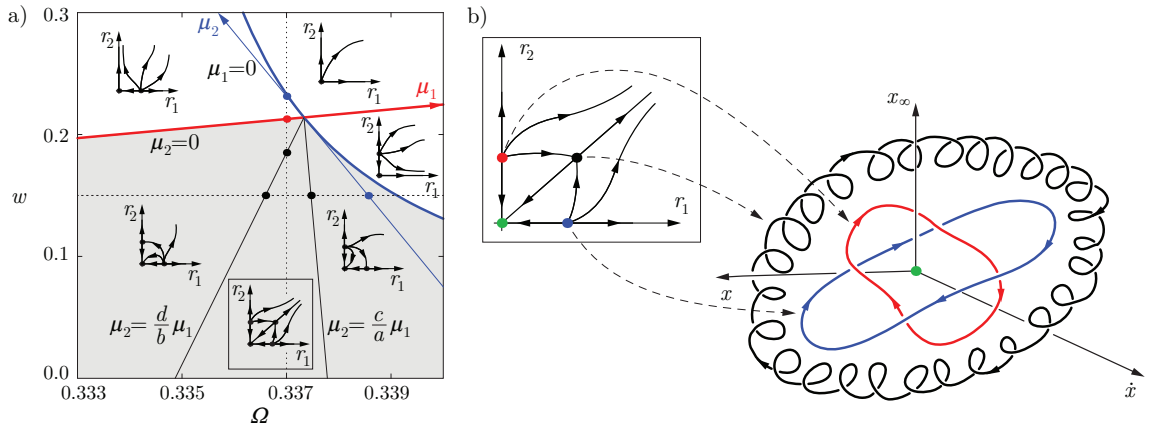

Fig. 2. Topology of the simplified two-dimensional phase portraits (a); its interpretation in the infinite-dimensional state space (b).

and $A < 0$ for all other double Hopf points. Based on the coefficients a, b, c, d, A, and the bifurcation parameters Ω, w, different topologies can be observed in simplified phase portraits depicted in two dimensions along (r_1, r_2). The possible topologies are discussed in [25]. Case Ia of the book by Guckenheimer and Holmes [25] applies for the first double Hopf point, and case Ib for all others.

Fig. 2(a) shows the simplified phase portraits at the third double Hopf point (at the intersection of the third and the fourth lobe). According to [25], the lines $\mu_1 = 0$, $\mu_2 = 0$ approximate the Hopf lobes (indicated by blue and red), where periodic solutions are born. In the simplified phase portraits, these periodic solutions are represented by the equilibrium points $(r_1^{\mathrm{p}}, 0)$ and $(0, r_2^{\mathrm{p}})$, respectively. Whereas lines $\mu_2 = c\mu_1/a$ and $\mu_2 = d\mu_1/b$ are the approximations of torus bifurcation branches (shown by black), where a quasi-periodic solution represented by $(r_1^{\mathrm{qp}}, r_2^{\mathrm{qp}})$ is born from one of the periodic solutions $((r_1^{\mathrm{p}}, 0)$ or $(0, r_2^{\mathrm{p}})$, respectively). The amplitude of these solutions is given by

$$
\begin{aligned}
r_1^{\mathrm{p}}(\hat{w}, \hat{\Omega}) &= \sqrt{-\frac{\gamma_{11}\hat{w} + \gamma_{12}\hat{\Omega}}{a_{11}}}, \quad & r_1^{\mathrm{qp}}(\hat{w}, \hat{\Omega}) &= \sqrt{\frac{(a_{12}\gamma_{21} - a_{22}\gamma_{11})\,\hat{w} + (a_{12}\gamma_{22} - a_{22}\gamma_{12})\,\hat{\Omega}}{a_{11}a_{22} - a_{12}a_{21}}}, \\
r_2^{\mathrm{p}}(\hat{w}, \hat{\Omega}) &= \sqrt{-\frac{\gamma_{21}\hat{w} + \gamma_{22}\hat{\Omega}}{a_{22}}}, \quad & r_2^{\mathrm{qp}}(\hat{w}, \hat{\Omega}) &= \sqrt{\frac{(a_{21}\gamma_{11} - a_{11}\gamma_{21})\,\hat{w} + (a_{21}\gamma_{12} - a_{11}\gamma_{22})\,\hat{\Omega}}{a_{11}a_{22} - a_{12}a_{21}}}.
\end{aligned}
\tag{20}
$$

The interpretations of the two-dimensional simplified phase portraits is shown in Fig. 2(b). The equilibria $(0, 0)$, $(r_1^{\mathrm{p}}, 0)$, $(0, r_2^{\mathrm{p}})$, and $(r_1^{\mathrm{qp}}, r_2^{\mathrm{qp}})$ correspond to the trivial equilibrium, to two periodic solutions, and to the quasi-periodic

Table 1. Bifurcation parameters, chatter frequencies, root tendencies, and normal form coefficients at the double Hopf points.

j_1	j_2	ω_1	ω_2	Ω_{dH}	w_{dH}	γ_{11}	γ_{12}	γ_{21}	γ_{22}
1	2	1.00060	1.52994	1.01018	0.671754	0.005553	0.3623	0.2963	−0.6699
2	3	1.00127	1.27729	0.505718	0.317804	0.01294	0.7071	0.3264	−1.006
3	4	1.00189	1.19274	0.337335	0.214010	0.01917	1.000	0.3263	−1.290
4	5	1.00247	1.15031	0.253092	0.164877	0.02429	1.251	0.3182	−1.530
5	6	1.00301	1.12474	0.202528	0.136344	0.02849	1.466	0.3074	−1.736

j_1	j_2	a_{11}	a_{12}	a_{21}	a_{22}	a	b	c	d	A	b_{num}	c_{num}
1	2	8.090×10^{-6}	0.008128	0.0002925	0.4317	1	0.01883	36.16	1	0.3193	0.01883	36.16
2	3	3.980×10^{-5}	0.01280	0.0009766	0.2239	1	0.05716	24.54	1	−0.4026	0.05721	24.51
3	4	8.807×10^{-5}	0.01479	0.001696	0.1500	1	0.09856	19.26	1	−0.8980	0.09855	19.26
4	5	1.460×10^{-4}	0.01560	0.002356	0.1121	1	0.1392	16.14	1	−1.248	0.1392	16.14
5	6	2.089×10^{-4}	0.01586	0.002939	0.08900	1	0.1782	14.07	1	−1.507	0.1782	14.07

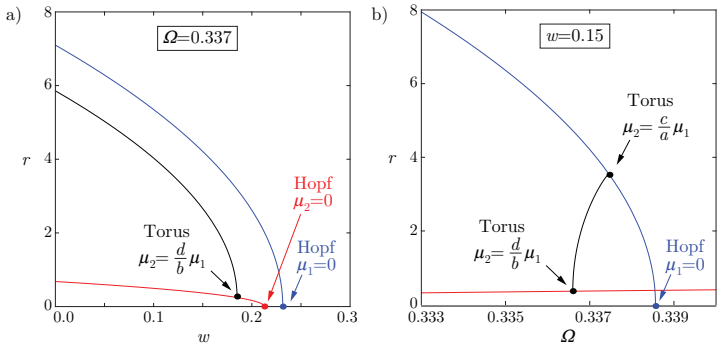

Fig. 3. Bifurcation diagrams near the double Hopf point as a function of the chip width w (a); as a function of the spindle speed Ω (b).

solution, respectively, in the infinite-dimensional phase space of the original time-delay system. For the sake of a simple illustration, the infinite-dimensional phase portrait is represented by a three-dimensional one in Fig. 2(b) using axes x, $\dot{x}$, and x_∞. Here, x_∞ stands for the remaining infinite dimensions, and x_∞ has no physical meaning, since it is introduced for illustration purposes only. Therefore, only the qualitative behavior and not the actual (infinite-dimensional) solutions are shown in the figure.

Finally, Fig. 3 shows the amplitude $r = r_1 + r_2$ of the arising periodic and quasi-periodic solutions according to Eq. (20) as a function of the bifurcation parameters Ω and w. The bifurcation diagrams are computed for $\Omega = 0.337$ and $w = 0.15$ as shown by the dotted lines in Fig. 2(a). The solutions related to $(r_1^{\mathrm{p}}, 0)$, $(0, r_2^{\mathrm{p}})$, and $(r_1^{\mathrm{qp}}, r_2^{\mathrm{qp}})$ are shown by blue, red, and black colors, respectively. Hopf bifurcations are indicated in Fig. 3(a), where the periodic solutions are born when decreasing w. A torus bifurcation point can also be seen, where the quasi-periodic solution is born from the periodic solution related to $(0, r_2^{\mathrm{p}})$. These bifurcation points are also indicated by dots in Fig. 2(a). In Fig. 3(b), two torus bifurcation points can be observed. When increasing Ω, the quasi-periodic solution is born from the periodic solution related to $(0, r_2^{\mathrm{p}})$, and then it vanishes by colliding with the periodic solution of $(r_1^{\mathrm{p}}, 0)$. Note that the bifurcation diagrams in Fig. 3 are not valid at large amplitudes due to loss of contact between the tool and the workpiece. When loss of contact occurs, Eq. (1) becomes no longer valid and the periodic solutions disappear[9]. Similarly, we expect the quasi-periodic solution to vanish at loss of contact. Locating the point where the tool loses contact is out of scope of this paper, but we remark that it has an important role in determining the global stability boundaries of the equilibrium.

Acknowledgements

This work has been supported by the ÚNKP-16-3-I. New National Excellence Program of the Ministry of Human Capacities. This work has received funding from the János Bolyai Research Scholarship of MTA (BO/00589/13/6). This work was supported by the Hungarian National Science Foundation under grant OTKA-K105433. The research leading to these results has received funding from the European Research Council under the European Union's Seventh Framework Programme (FP/2007-2013) / ERC Advanced Grant Agreement n. 340889.

Appendix A. An example appendix

The auxiliary parameters used in the paper are

$$V_{1,2} = \cos(\omega_{1,2}\tau_{\mathrm{dH}}) - 1\,, \quad W_{1,2} = -\sin(\omega_{1,2}\tau_{\mathrm{dH}})\,, \quad p_{1,2} = 2\zeta + \tau_{\mathrm{dH}}\left(1 + w_{\mathrm{dH}} - \omega_{1,2}^2\right), \quad q_{1,2} = 2\omega_{1,2}\left(1 + \zeta\tau_{\mathrm{dH}}\right),$$
$$R_{1,2} = 1 - \cos(2\omega_{1,2}\tau_{\mathrm{dH}})\,, \quad S_{1,2} = \sin(2\omega_{1,2}\tau_{\mathrm{dH}})\,, \quad R_{3,4} = 1 - \cos((\omega_2 \pm \omega_1)\tau_{\mathrm{dH}})\,, \quad S_{3,4} = \sin((\omega_2 \pm \omega_1)\tau_{\mathrm{dH}})\,,$$
$$K_{1,2} = wR_{1,2} - \left(4\omega_{1,2}^2 - 1\right), \; L_{1,2} = wS_{1,2} + 4\zeta\omega_{1,2}\,, \; K_{3,4} = wR_{3,4} - \left((\omega_2 \pm \omega_1)^2 - 1\right), \; L_{3,4} = wS_{3,4} + 2\zeta(\omega_2 \pm \omega_1)\,. \tag{A.1}$$

The expressions of the cubic normal form coefficients read

$$
\begin{aligned}
a_{11} =& -\frac{1}{2}w^2(V_1^2+W_1^2)\eta_2^2\left(\frac{K_1R_1+L_1S_1}{K_1^2+L_1^2}\frac{p_1V_1+q_1W_1}{p_1^2+q_1^2}+\frac{K_1S_1-L_1R_1}{K_1^2+L_1^2}\frac{q_1V_1-p_1W_1}{p_1^2+q_1^2}\right)+\frac{3}{4}w(V_1^2+W_1^2)\eta_3\frac{p_1V_1+q_1W_1}{p_1^2+q_1^2}\,,\\
a_{12} =& -w^2(V_2^2+W_2^2)\eta_2^2\left(\left(\frac{K_3R_3+L_3S_3}{K_3^2+L_3^2}+\frac{K_4R_4+L_4S_4}{K_4^2+L_4^2}\right)\frac{p_1V_1+q_1W_1}{p_1^2+q_1^2}\right.\\
&\left.+\left(\frac{K_3S_3-L_3R_3}{K_3^2+L_3^2}-\frac{K_4S_4-L_4R_4}{K_4^2+L_4^2}\right)\frac{q_1V_1-p_1W_1}{p_1^2+q_1^2}\right)+\frac{3}{2}w(V_2^2+W_2^2)\eta_3\frac{p_1V_1+q_1W_1}{p_1^2+q_1^2}\,,
\end{aligned}
\tag{A.2}
$$

whereas a_{21} and a_{22} can be obtained by interchanging ω_1 and ω_2 in the formulas of a_{12} and a_{11}, respectively.

References

1. Tobias, S.A., Fishwick, W.. Theory of regenerative machine tool chatter. *The Engineer* 1958;:199–203, 238–239.
2. Tlusty, J., Polacek, M.. The stability of the machine tool against self-excited vibration in machining. In: *ASME Production Engineering Research Conference*. Pittsburgh; 1963, p. 454–465.
3. Shi, H.M., Tobias, S.A.. Theory of finite amplitude machine tool instability. *Int J Mach Tool D R* 1984;**24**(1):45–69.
4. Endres, W.J., Loo, M.. Modeling cutting process nonlinearity for stability analysis - application to tooling selection for valve-seat machining. In: *5th CIRP International Workshop on Modeling of Machining*. West Lafayette, IN, USA; 2002, p. 71–82.
5. Ahmadi, K., Ismail, F.. Experimental investigation of process damping nonlinearity in machining chatter. *Int J Mach Tool Manu* 2010; **50**(11):1006–1014.
6. Altintas, Y.. *Manufacturing Automation - Metal Cutting Mechanics, Machine Tool Vibrations and CNC Design, Second Edition*. Cambridge: Cambridge University Press; 2012.
7. Hale, J.. *Theory of Functional Differential Equations*. New York: Springer; 1977.
8. Stépán, G., Kalmár-Nagy, T.. Nonlinear regenerative machine tool vibrations. In: *Proc of DETC'97, ASME Design and Technical Conferences*. Sacramento, CA, USA; 1997, p. 1–11.
9. Dombóvári, Z., Wilson, R.E., Stépán, G.. Estimates of the bistable region in metal cutting. *P Roy Soc Lond A-Math Phy* 2008;**464**:3255–3271.
10. Nayfeh, A.H., Mook, D.T.. *Nonlinear Oscillations*. New York: Wiley; 1979.
11. Nayfeh, A.H.. Order reduction of retarded nonlinear systems – the method of multiple scales versus center-manifold reduction. *Nonlinear Dynam* 2008;**51**(4):483–500.
12. Nandakumar, K., Wahi, P., Chatterjee, A.. Infinite dimensional slow modulations in a well known delayed model for cutting tool vibrations. *Nonlinear Dynam* 2010;**62**(4):705–716.
13. Engelborghs, K., Luzyanina, T., Roose, D.. Numerical bifurcation analysis of delay differential equations using DDE-BIFTOOL. *ACM T Math Software* 2002;**28**(1):1–21.
14. Campbell, S.A., Bélair, J., Ohira, T., Milton, J.. Limit cycles, tori, and complex dynamics in a second-order differential equation with delayed negative feedback. *J Dynam Differential Equations* 1995;**7**(1):213–236.
15. Stépán, G.. Modelling nonlinear regenerative effects in metal cutting. *P Roy Soc A-Math Phy* 2001;**359**(1781):739–757.
16. Xu, J., Chung, K.W., Chan, C.L.. An efficient method for studying weak resonant double Hopf bifurcation in nonlinear systems with delayed feedbacks. *SIAM J Appl Dyn Syst* 2007;**6**(1):29–60.
17. Guo, S., Chen, Y., Wu, J.. Two-parameter bifurcations in a network of two neurons with multiple delays. *J Differ Equations* 2008; **244**(2):444–486.
18. Ma, S., Lu, Q., Feng, Z.. Double Hopf bifurcation for Van der Pol-Duffing oscillator with parametric delay feedback control. *J Math Anal Appl* 2008;**338**(2):993–1007.
19. Wang, W., Xu, J.. Multiple scales analysis for double Hopf bifurcation with 1:3 resonance. *Nonlinear Dynam* 2011;**66**(1):39–51.
20. Bazsó, C., Champneys, A.R., Hős, C.J.. Bifurcation analysis of a simplified model of a pressure relief valve attached to a pipe. *SIAM J Appl Dyn Syst* 2014;**13**(2):704–721.
21. Qesmi, R., Babram, M.A.. Double Hopf bifurcation in delay differential equations. *Arab J Math Sci* 2014;**20**(2):280–301.
22. Shen, Z., Zhang, C.. Double hopf bifurcation of coupled dissipative Stuart-Landau oscillators with delay. *Appl Math Comput* 2014; **227**:553–566.
23. Ding, Y., Cao, J., Jiang, W.. Double hopf bifurcation in active control system with delayed feedback: application to glue dosing processes for particleboard. *Nonlinear Dynam* 2016;**83**(3):1567–1576.
24. Wahi, P., Chatterjee, A.. Regenerative tool chatter near a codimension 2 Hopf point using multiple scales. *Nonlinear Dynam* 2005; **40**(4):323–338.
25. Guckenheimer, J., Holmes, P.. *Nonlinear Oscillations, Dynamical Systems, and Bifurcations of Vector Fields*. New York: Springer; 1983.
26. Knobloch, E.. Normal form coefficients for the nonresonant double Hopf bifurcation. *Phys Lett A* 1986;**116**(8):365–369.